Journal of Neurochemistry

JOURNAL OF NEUROCHEMISTRY | 2018 | 144 | 390–407 doi: 10.1111/jnc.14254

ORIGINAL ARTICLE

Protein components of post-synaptic density lattice, a backbone structure for type I excitatory synapses

Tatsuo Suzuki,*·†·‡ Kiyokazu Kametani,§ Weiheng Guo* and Weidong Li¶·**

*Department of Neuroplasticity, Institute of Pathogenesis and Disease Prevention, Graduate School of Medicine, Shinshu University Academic Assembly, Matsumoto, Japan

†Department of Biological Sciences for Intractable Neurological Diseases, Institute for Biomedical Sciences, Interdisciplinary Cluster for Cutting Edge Research Shinshu University, Matsumoto, Japan

‡Department of Molecular and Cellular physiology, Shinshu University Academic Assembly, Institute of Medicine, Matsumoto, Japan

§Department of Instrumental Analysis, Research Center for Human and Environmental Science, Shinshu University, Matsumoto, Nagano, Japan

¶Bio-X Institutes, Key Laboratory for the Genetics of Development and Neuropsychiatric Disorders (Ministry of Education), Shanghai Key Laboratory of Psychotic Disorders, and Brain Science and Technology Research Center, Shanghai Jiao Tong University, Shanghai, China

**Distinguished Visiting Professor, Institute for Biomedical Sciences, Interdisciplinary Cluster for Cutting Edge Research Shinshu University, Matsumoto, Japan

Abstract

It is essential to study the molecular architecture of post-synaptic density (PSD) to understand the molecular mechanism underlying the dynamic nature of PSD, one of the bases of synaptic plasticity. A well-known model for the architecture of PSD of type I excitatory synapses basically comprises of several scaffolding proteins (scaffold protein model). On the contrary, 'PSD lattice' observed through electron microscopy has been considered a basic backbone of type I PSDs. However, major constituents of the PSD lattice and the relationship between the PSD lattice and the scaffold protein model, remain unknown. We purified a PSD lattice fraction from the synaptic plasma membrane of rat forebrain. Protein components of the PSD lattice were examined through immuno-gold negative staining electron microscopy. The results indicated that tubulin, actin, α-internexin, and Ca^{2+}/calmodulin-dependent kinase II are major constituents of the PSD lattice, whereas scaffold proteins such as PSD-95, SAP102, GKAP, Shank1, and Homer, were rather minor components. A similar structure was also purified from the synaptic plasma membrane of forebrains from 7-day-old rats. On the basis of this study, we propose a 'PSD lattice-based dynamic nanocolumn' model for PSD molecular architecture, in which the scaffold protein model and the PSD lattice model are combined and an idea of dynamic nanocolumn PSD subdomain is also included. In the model, cytoskeletal proteins, in particular, tubulin, actin, and α-internexin, may play major roles in the construction of the PSD backbone and provide linker sites for various PSD scaffold protein complexes/subdomains.

Keywords: molecular architecture, post-synaptic density, PSD lattice, synaptic plasticity, type I synapse.

J. Neurochem. (2018) **144**, 390–407.

Received September 11, 2017; revised manuscript received October 17, 2017; accepted November 1, 2017.

Address correspondence and reprint requests to Tatsuo Suzuki, Department of Molecular and Cellular physiology, Shinshu University, 3-1-1 Asahi, Matsumoto 390-8621, Japan. E-mail: suzukit@shinshu-u.ac.jp

Abbreviations used: CaMKII, Ca^{2+}/calmodulin-dependent protein kinase II; CaMKIIα, α subunit of CaMKII; CaMKIIβ, β subunit of CaMKII; DOC, deoxycholate; EM, electron microscope, electron microscopy, or electron microscopic; IAA, iodoacetamide; MAGUK, membrane-associated guanylate kinase; NF-L, neurofilament-L; OG, n-Octyl-β-D-glucoside; PSD, post-synaptic density; SDG, sucrose density gradient; SPM, synaptic plasma membrane; TX, TritonX-100; α-IN, α-internexin.

Post-synaptic density (PSD) plays important roles in signal processing upon receiving the neurotransmitter, which is related to generating synaptic plasticity. The shape and size of PSD, as well as the spine, change when long-term potentiation or long-term depression is induced (Bosch *et al.* 2014). PSD is approximately 1 GDa (giga Dalton), which consists of several hundred to a thousand types of proteins. Membrane-associated guanylate kinase (MAGUK)-organized model (we refer to this as 'scaffold protein model' hereafter) for molecular architecture of the type I excitatory PSD has been discussed in recent years (Kim and Sheng 2004; Boeckers 2006; Feng and Zhang 2009). In this model, the basic structure of the type I PSD is constructed by various scaffold proteins, many of which were found after the middle 1990′s. Among the scaffold proteins in the PSD, Shank/ProSAP family protein is considered one of master scaffold proteins in the PSD, and nucleate underlying structure of the PSD (Baron *et al.* 2006). In a recent concept (Dosemeci *et al.* 2016), PSD is divided into two areas: 'PSD core' and 'PSD pallium', of which the depths are typically 30–50 nm from the post-synaptic membrane and further 50–60 nm toward the cytoplasmic side, respectively. The 'PSD core' is constantly highly electron-dense and corresponds to the surface area and the second layer immediately beneath the post-synaptic membrane where Glutamate receptors, PSD-95, and GKAP are localized. The PSD pallium is an area where Homer is localized and Ca^{2+}/calmodulin-dependent protein kinase II (CaMKII), synGAP, AIDA, and Shank translocate and become electron-dense when the synapse is intensely activated. Purified PSD contains not only 'PSD core' but also PSD pallium. There are actin-based cytoskeletons expanding from the PSD pallium to the cytoplasm of the spine.

Very early electron microscopic (EM) studies, before the discovery of a number of PSD scaffold proteins, revealed that PSD consists of a filamentous network, and the structure is called the 'filamentous web of the PSD' or 'dense submembranous filamentous array' (Blomberg *et al.* 1977; Cohen *et al.* 1983). The fibrous structure in the spine and PSD is also observable in the deep etched freeze fractured samples (Landis and Reese 1983; Hirokawa 1989). Furthermore, a network structure, which was called 'junctional lattice' or 'PSD lattice' has been identified by extraction of synaptic plasma membrane (SPM), synaptic junction, or TritonX-100 (TX)-insoluble PSD with relatively strong detergent, deoxycholate (DOC), and proposed to be an underlining structure of the PSD (Matus and Walters 1975; Blomberg *et al.* 1977; Matus and Taff-Jones 1978; Matus 1981). The PSD lattice is composed of a branching network of 5-nm-thick fibers, which construct an array of polygonal holes, each polygon being approximately 20 nm across. The PSD is elaborated on the lattice framework (PSD lattice). A mesh-like structure, similar to the PSD lattice, was also indicated in the platinum-shadowed adult PSDs (Petersen *et al.* 2003), and in the purified immature and mature PSD by electron cryotomography (Swulius *et al.* 2012). Till now the key components and molecular organization of the PSD lattice have not yet been clarified because DOC-insoluble PSD containing the PSD lattice still contains numerous proteins, as well as TX-insoluble PSDs (Blomberg *et al.* 1977; Matus and Taff-Jones 1978). It is currently tacitly believed that various kinds of scaffold proteins are interwoven to make the lattice-like network structure of PSD.

A recent study suggested the importance of post-synaptic structural remodeling for long-term potentiation expression, whereby the remodeling consisted of two steps: spine and PSD remodeling (Bosch *et al.* 2014). The molecular mechanism underlying the PSD remodeling is not known at present. Precise knowledge of the PSD structure is indispensable for a deep understanding of the molecular mechanism for spine and PSD dynamics during expression of synaptic plasticity. In this paper, we investigated the basic backbone structure of type I excitatory PSD. In particular, it remains unclear whether the PSD lattice is a structure woven mainly, or only, by various PSD scaffold proteins. We examined the protein components of a purified PSD lattice structure through immuno-gold negative staining electron microscopy (EM).

Materials and methods

This study was not pre-registered.

Materials

Chemicals and antibodies used in this study are listed in Tables 1 and 2. All chemicals not listed in the Table 1 are of reagent grade.

Ethical approval/animals

Animals were handled in accordance with the Regulations for Animal Experimentation of Shinshu University. The animal protocol, together with animals handling, was approved by the Committee for Animal Experiments of Shinshu University (Approval Number 240066). Based on the national regulations and guidelines, all experimental procedures were reviewed by the Committee for Animal Experiments and finally approved by the president of Shinshu University.

Pregnant rats (Slc:Wistar(SPF), RRID, RGD_2314928, body weight: 220–250 g) were purchased from Japan SLC, Inc. (Hamamatsu, Japan) and housed at 23 ± 3°C, constant humidity, and 12-h light/dark cycle, in flat floor cage made by resin (polysulfone) with paper chip. Animals had free access to tap water and standard rat chow.

Preparation of SPMs, regular TX-PSD, and DOC-PSD

SPMs were prepared from Wistar rats (male, 6 weeks old, body weight: 150 ± 8 g or 7-days old, body weight: 15 ± 1.2 g and 14.5 ± 0.8 g for male and female, respectively, specific-pathogen-free) (Japan SLC, Inc.), as described previously (Suzuki 2011). To

Table 1 List of major chemicals used in this study

Chemicals (abbreviated names)	Code No.	RRIDs	Providers
TritonX-100 (TX-100)	581-81705	Not found	WAKO Pure Chemical Industries. Ltd. (Osaka, Japan)
Iodoacetamide (IAA)	095-02891	Not found	WAKO Pure Chemical Industries. Ltd. (Osaka, Japan)
Deoxycholate (DOC)	192-08312	Not found	WAKO Pure Chemical Industries, Ltd. (Osaka, Japan)
ImmunoStar LD	292-69903	Not found	WAKO Pure Chemical Industries. Ltd. (Osaka, Japan)
n-Octyl-β-D-glucoside (OG)	346-05033	Not found	Dojindo Laboratories (Kumamoto, Japan)
Nano-W	2018	Not found	Molecular probes (Yaphank, NY, USA)
Protease inhibitor cocktail	P8340	Not found	Sigma-Aldrich (St Louis, MO, USA)
Pepsin	S3002	Not found	DAKO (Carpinteria, CA, USA)
Silver staining kit	AE-1360	Not found	ATTO (Atto Bioscience & Biotechnology) (Tokyo, Japan)
SYPRO Ruby Protein Blot Stain	50565	Not found	Lonza Rockland, Inc. (Rockland, ME, USA)

prevent artificial oxidative cross-linking of proteins during the preparation of SPMs, buffers A and B were supplemented with 2 mM iodoacetamide (IAA) during the isolation process. Purified SPMs were stored unfrozen in buffers containing 50% glycerol at −30°C. Longer storage at −80°C did not cause any deterioration of the samples in this experiment.

'Regular' TX-PSD (PSD prepared by TX-100 treatment; similar designation to follow throughout) was prepared from 6-week-old rat forebrains, using the method of Cohen *et al.* (Suzuki 2011). DOC-PSD holding the 'authentic' PSD lattice structure was prepared by treatment of regular TX-PSD with 0.5% DOC for 1 h at 4°C and pelleted by centrifugation at 15 800 *g* for 5 min at 4°C, using the method by Blomberg *et al.* (1977).

Purification of 1% n-Octyl-β-D-glucoside (OG)-IS-11, 1% OG-IS-11B, and OG-PSD

Purification of fractions after sucrose density gradient (SDG) centrifugation is summarized in Figure S1. SPMs (500 μg protein, small-scale purification) was treated with 1% n-Octyl-β-D-glucoside (OG) in 1.75 mL of 20 mM Tris–HCl buffer (pH 7.4) containing 150 mM NaCl and 1 mM EDTA (TNE buffer), and separated into the soluble and pellet fractions by ultracentrifugation at 200 000 g_{max} for 30 min at 4°C. Detergent treatments were supplemented with protein inhibitor mixtures (p8340; Sigma-Aldrich, St Louis, MO, USA) at 1/200 dilution, along with IAA (2 mM). The pellets (insoluble fraction, IS) were hand-homogenized with Hamilton homogenizer, in 1.75 mL of TNE buffer, supplemented with IAA (2 mM), mixed with an equal volume of TNE containing 80% sucrose, and poured into centrifuge tubes. The solutions were overlaid with TNE buffers containing 30% sucrose and then 5% sucrose (3.5 mL each), and centrifuged at 256 000 g_{max} for 30 h at 4°C. Eleven fractions were collected and the pellets (fraction 12) were suspended with 955 μL of TNE buffer. 1% OG-IS-11 is the 11th fraction (an insoluble fraction 11 obtained after treatment with 1% OG; similar designation to follow throughout).

The PSD lattice fraction, a bottom portion of 1% OG-IS-11 (1% OG-IS-11B) was isolated from SPMs (5 mg, large-scale purification) after treatment with 1% OG in 17.5 mL of TNE buffer. Because concentration of PSD lattice structures contained in the 1% OG-IS-11B is low, it is necessary to purify it by a large-scale method, as mentioned here. The pellets obtained after the ultracentrifugation were hand-homogenized in 1.75 mL of TNE buffer, and processed for the SDG centrifugation as described above. 1% OG-IS-11B is a bottom portion (~ 100 μL) of 1% OG-IS-11. For OG-PSD, we recovered pellet/fraction-12 after the SDG. In some cases, for PSD purification, ultracentrifugation before SDG centrifugation was omitted for easiness. Therefore, OG-PSD was prepared as either OG-12 or OG-IS-12, and the detailed fraction name was supplemented in parenthesis after each OG-PSD. The OG-12 PSD contains exclusively type I excitatory PSD (Zhao *et al.* 2014).

Immuno-gold negative staining and EM

Thin section samples for EM were prepared as described previously (Suzuki *et al.* 2011). Briefly, sample solution containing 1% OG-insolubule structures was incubated with 2% glutaraldehyde for 1 h, and further incubated with 1% osmiumtetroxide for 30 min, both on ice. Pellets were obtained by centrifugation at 15 800 *g* for 2 min at 4°C, dehydrated with series of graded concentrations of ethanol, transferred into propylene oxide, and embedded in Epon. An ultrathin section was cut and stained with uranyl acetate and lead citrate.

For negative staining coupled with immuno-gold technique, 5-nm or 10-nm gold particles (less than 12 nm) were used (DeGiorgis *et al.* 2006). Structures in the 1% OG-IS-11B or PSD preparation (1% OG-IS-12 in this case), in a solution supplemented with 1/200-diluted protease inhibitor cocktail, were attached to the formvar-coated grid at 0°C. The formvar membrane on the gird was blocked with 10% normal goat or rabbit serum in Tris-buffered saline (TBS) (pH 7.4) on ice for 10 min, followed by 5% bovine serum albumin (BSA) in TBS (twice), incubated with the 1st antibody (Table 2) suspended in the 1% normal goat or rabbit serum at 25°C for 1 h, washed with 5% BSA in TBS three times, further incubated with immuno-gold-labeled anti-mouse, rabbit or goat antibody (1/50-diluted in the 1% normal goat or rabbit serum) at 25°C for 30 min, fixed with 1% glutaraldehyde in phosphate-buffered saline (PBS) for 5 min on ice, and washed with H_2O three times briefly. Then, the samples were negatively stained with nano-W (methylamine tungstate) twice following the manufacturer's recommendation. Incubation with the 1st and 2nd antibodies was carried out in the presence of a protease inhibitor cocktail at 1/200 dilution. In some cases, samples were treated with pepsin at 35°C for an indicated time, after blocking with 10% normal goat or rabbit serum. The

Table 2 List of antibodies used for immuno-gold electron microscopy

Antibodies used for immuno-gold labeling	RRID (–), not found or no exact match	Catalog or clone No.	Company	Mono or poly	Animals for antibody production	Dilution used
Anti-tubuin	Not registered	(1)	Produced by Dr. Fujii, Shinshu University	Polyclonal	Rabbit	1/20
Anti-β-tubulin	(–)	T-5201	Sigma (Saint Louis, MO, USA)	Monoclonal	Mouse	1/20
Anti-β-actin[a]	AB_626632	sc-47778	Santa Cruz Biotechnology Inc. (Santa Cruz, CA, USA)	Monoclonal	Mouse	1/20
Anti-α-Internexln	AB_91800	AB5354	Chemicon International (Billerica, MA, USA)	Polyclonal	Rabbit	1/50
Anti-neurofilament L	AB_1555280	DA2	Novus Biologicals (Littleton, CO, USA)	Monoclonal	Mouse	1/20
Anti-CaMKIIα	(–)	6G9	Chemicon International	Monoclonal	Mouse	1/20
Anti-CaMKIIβ	(–)	3232SA	Gibco BRL (Gaithersburg, MD, USA)	Monoclonal	Mouse	1/20
Anti-PSD-95	(–)	MA1 -045	ABR (Golden, CO, USA)	Monoclonal	Mouse	1/20
Anti-SAP102	AB_2261666	N19/2	UC Davls/NIH NeuroMab facility (Davis, CA, USA)	Monoclonal	Mouse	1/20
Anti-shank1	AB_2270283	N22/21	UC Davls/NIH NeuroMab facility	Monoclonal	Mouse	1/20
Anti-GKAP (Pan-SAPAP)	ABJ0671947	N127/31	UC Davls/NIH NeuroMab facility	Monoclonal	Mouse	1/20
Anti-Homer	AB_648368	sc-8921	Santa Cruz Biotechnology Inc.	Polyclonal	Goat	1/20
Anti-Homer 1	AB_1950505	GTX103278	GeneTex, Inc. (Irvine, CA, USA)	Polyclonal	Rabbit	1/20
Anti-Homer 3	AB_10621284	GTX 115242	Gen eTex, Inc.	Polyclonal	Rabbit	1/20
Anti-mouse lgG(H+L)-gold label	(–)	EMGMHL5, EMGMHL10	BBI solutions (Cardiff, UK)	Polyclonal	Goat	1/50
Anti-rabbit lgG(H+L)-gold label	(–)	EMGAR5, EMGAR10	BBI solutions	Polyclonal	Goat	1/50
Anti-goat lgG(H+L)-gold label	(–)	EMRAG10	BBI solutions (Cardiff, UK)	Polyclonal	Rabbit	1/50

(1) Anti-tubulin antibody was produced in a rabbit using pig tubulin as antigen.

[a]Anti-β-actin (sc-47778; Santa Cruz Biotechnology Inc., Santa Cruz, CA, USA) was used, because anti-pan-actin antibody (pan Ab-5; Thermo scientific, UK, RRID, AB_10983629) did not label well the 1% OG-11B and PSD.

pepsin treatment was stopped immediately by transfer of the grid onto H_2O droplet twice, followed on by cold TBS containing 5% BSA solution. Optimum durations of pepsin pre-treatment were determined sample to sample and antibody to antibody.

Specimens were examined under a JEOL JEM-1400EX electron microscope (EM) (JEOL, Tokyo, Japan) at 80 kV and images were taken by 4008 × 2672 pixel elements CCD camera (Gatan SC1000; Gatan Inc., Tokyo, Japan). Stereo pair images were made from two images obtained after tilting at +10° to −10° with a goniometer stage, using the tilting device of the JEM-1400 microscopes. For EM tomography, the specimen (thin sections of 1% OG-IS-11) was tilted from −60° to + 60° and imaged at 1° steps (121 images per view). Images were taken by RECORDER Roku Software (System in Frontier, Inc., Tokyo, Japan) equipped with the JEOL JEM-1400EX EM. Images obtained from a tilt series were aligned using COMPOSER software (System in Frontier, Inc.), and three-dimensional (3-D) images were reconstructed using the simultaneous iterative reconstruction technique by VISUALIZER-Kai software (System in Frontier, Inc.). Sharpness of images was enhanced using Unsharp mask, and contrast of images was modified by Photoshop to demonstrate gold particles clearly. For quantification of PSD proteins, gold particles were counted after taking electron micrographs.

Protein profiling

For protein profiling, each SDG fraction (20 μL unless stated otherwise) was separated using sodium dodecyl sulfate–polyacrylamide gel electrophoresis (SDS–PAGE) and the gels were stained with silver or SYPRO Ruby. Western blotting was carried out using a chemiluminescent substrate and visualized with a CCD video camera system (Atto Densitograph Lumino CCD AE-6930; ATTO Bioscience & Technology, Tokyo, Japan). For dot blot, 2 μL of sample fraction was blotted on polyvinylidene difluoride membranes (Immobilon). Whole content of samples was blotted on the polyvinylidene difluoride membranes, without any solubilization or extraction. Blot membranes were then blocked with 0.5% BSA solution and processed for immunodetection in the same manner as western blotting.

Statistical analyses

Data are presented as mean ± SE. Vertical plots are indicated in the figures and Figure legends. The '*n*' number represents number of samples measured and is indicated in the parenthesis above each bar. Statistical analyses (Shapiro–Wilk normality test and Mann–Whitney test) were performed using GraphPad Prism version 6.0 (GraphPad Software, San Diego, CA, USA). Mann–Whitney test was adopted because samples were not in a normal distribution. No blinding and no randomization were performed. Results were taken to be statistically significant when $p < 0.05$.

Results

Morphology of the unique structures in 1% OG-IS-11 prepared from both adult and immature brains

We previously analyzed the separation process of synaptic membrane rafts and PSD from SPM, with three kinds of detergents (Zhao *et al.* 2014). In the study we found that OG solubilized most of the SPM proteins, except for actin, and left unique insoluble fraction, 1% OG-IS-11, which contained exclusively actin (Zhao *et al.* 2014) (See also Figure S2). We started to investigate if this fraction had structural elements for synapses. We identified mesh-like structures with various sizes (<1 μm) in the fraction. The structures were different from PSDs (Fig. 1b). Examples of enlarged individual mesh-like structures are shown in Fig. 1(c). Structures appeared to be relatively planar based on micrographs obtained from different angles (Fig. 1d-1 and d-2, Figure S3).

Furthermore, we observed the mesh-like structures by negative staining EM examination. Figure 2 shows stereo views of typical negatively stained structures. Fine appearance of molecules constructing mesh fibers was visualized. For observation of negatively stained samples, we used bottom portion of the 1% OG-IS-11 (1% OG-IS-11B) because structures of interest were more concentrated in the bottom portion.

We compared the morphology of the structures in the 1% OG-IS-11B with PSDs (1% OG-12 and 0.75% OG-12) in negative staining. Typical two photos for each preparation are shown in Fig. 3(a). The structures in the 1% OG-IS-11B appeared to be sparser than PSDs, and mesh-like structures (arrows in Fig. 3a) were more clearly observable than in the PSD. Similar but more packed structures were observed in 1% OG-PSD. In 0.75% OG-PSD, the structure was more packed with molecules and more electron-dense, than those in the 1% OG-PSD, which may be because of the milder solubilization with the lower concentration of OG. Similar difference in density of PSD was confirmed in thin sections (Figure S4). Sizes of the structures are in the same range between 1% OG-IS-11B and OG-PSDs. However, structures in the 1% OG-IS-11B were significantly, although to a small extent, smaller than 1% OG-PSDs (Fig. 3b). There was no significant difference in the size of mesh-like structures between thin sections and negative staining.

We then investigated the 1% OG-IS-11B fraction prepared from immature forebrains and compared it with immature PSDs (7 days, 1% OG-12) (Fig. 4 and Figure S4). Typical examples of stereo views of EM of negatively stained structures in the 7 days, 1% OG-IS-11, are shown in Figure S5. Immature PSD was sparser than the adult PSD in both negative staining and thin sections. Mesh-like structures were observed even in the PSD in thin section at 7 days of age (arrows in Fig. 4). Mesh-like structures similar to those in adult 1% OG-IS-11B, although not so clearly mesh-like, were observed in the negative staining of immature OG-IS-11B. Meager mesh-like structures, such as those shown in Fig. 4, were more frequent in the immature 1% OG-IS-11B than the adult ones.

Analysis of protein components of adult PSD lattice structure by immuno-gold negative staining EM

We examined distribution of typical PSD proteins in the mesh-like structures in the 1% OG-IS-11B by the immuno-gold EM technique, coupled with negative staining. We adopted this method because of the small requirement of samples and time to prepare EM samples. Also, direct detection of signals on the target structure can avoid false counts, owing to mixture with signals on the other structures co-existing in the preparation. We examined focusing on typical cytoskeletal and scaffold proteins in the PSD: tubulin, actin, α-internexin (α-IN), neurofilament-L (NF-L), CaMKIIα and β, PSD-95, SAP102, Shank1 GKAP/SAPAP, and Homer. Typical examples of distribution of immuno-gold labels for each protein in 1% OG-IS-11B are shown in Fig. 5(a) and Figure S6. For comparison, distribution was also examined in the same way in the 1% OG-PSD (1% OG-IS-12 in this case), and typical distributions are shown in Fig. 5b and Figure S7. There are no microtubules and only a few F-actin fibers associated with the structures in both 1% OG-IS-11B and 1% OG-PSD. Presence, abundance, and distribution of tubulin in the 1% OG-IS-11B, were confirmed on immuno-gold staining using another anti-tubulin antibody (anti-β-tubulin antibody (clone Tub2.1; Sigma, St Louis, MO, USA) (not shown).

We confirmed the results of immuno-gold negative staining by the immunogold labeling of the 'authentic PSD

Fig. 1 Electron microscopic observation of 1% n-Octyl-β-D-glucoside (OG)-IS-11B. Isolated 1%OG-IS-11B and OG-post-synaptic density (PSD) (0.75%OG-12) were fixed, embedded in Epon and thin sections were cut. Samples were stained with uranium acetate and lead citrate. (a) Low magnification of the 1%OG-IS-11B. (b) 0.75%OG-12. Typical PSD with horseshoe morphology is indicated with an arrow. (c) Magnified view of the structures identified in the 1%OG-IS-11B. (d-1 and d-2). Two images of EM tomography, which were obtained from different directions opened at 60°. See also three-dimensional reconstructions in Figure S3.

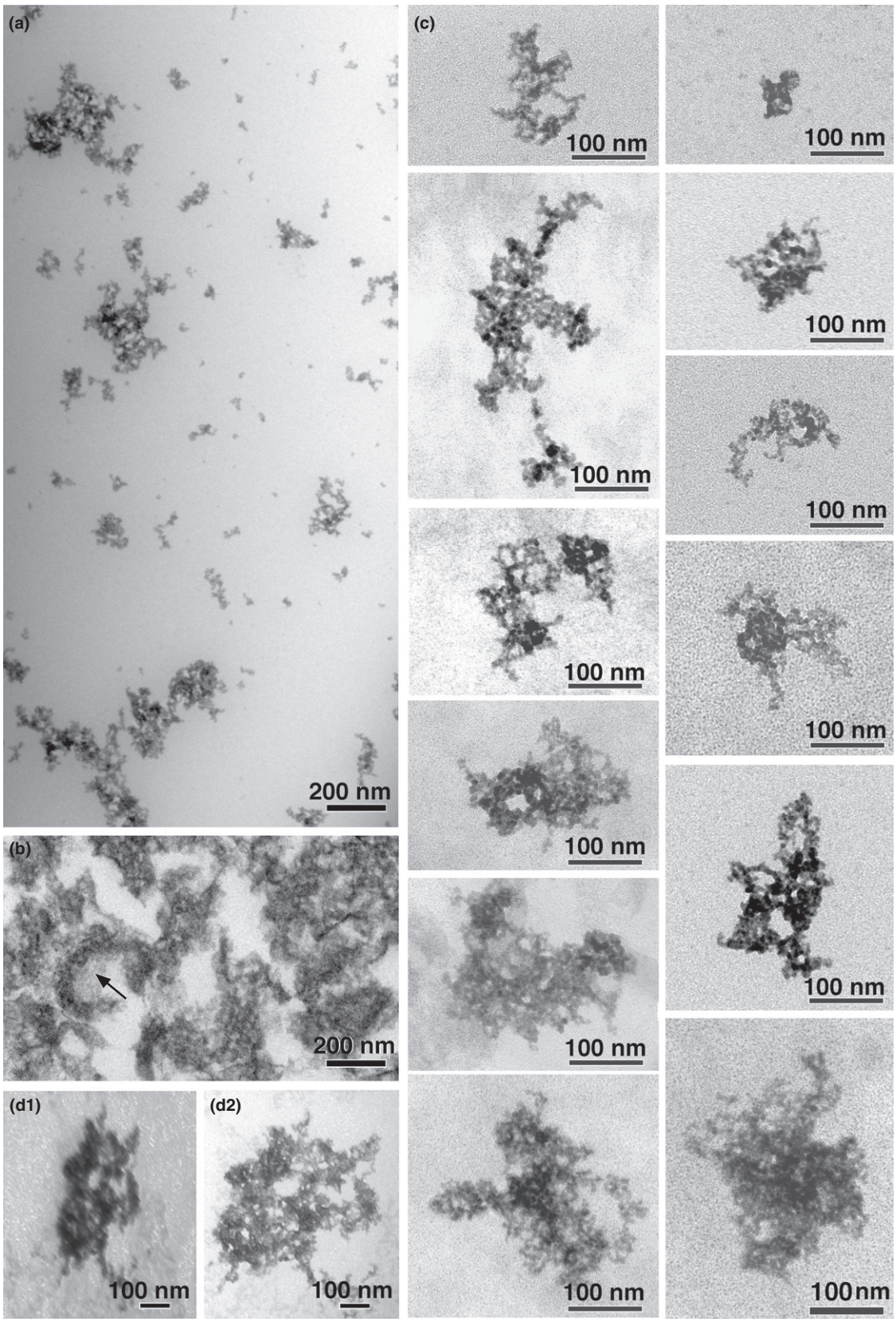
(a)
200 nm
(b)
200 nm
(d1)
100 nm
(d2)
100 nm
(c)
100 nm
100 nm
100 nm
100 nm
100 nm
100 nm
100 nm
100 nm
100 nm
100 nm
100 nm
100 nm
100 nm
100 nm

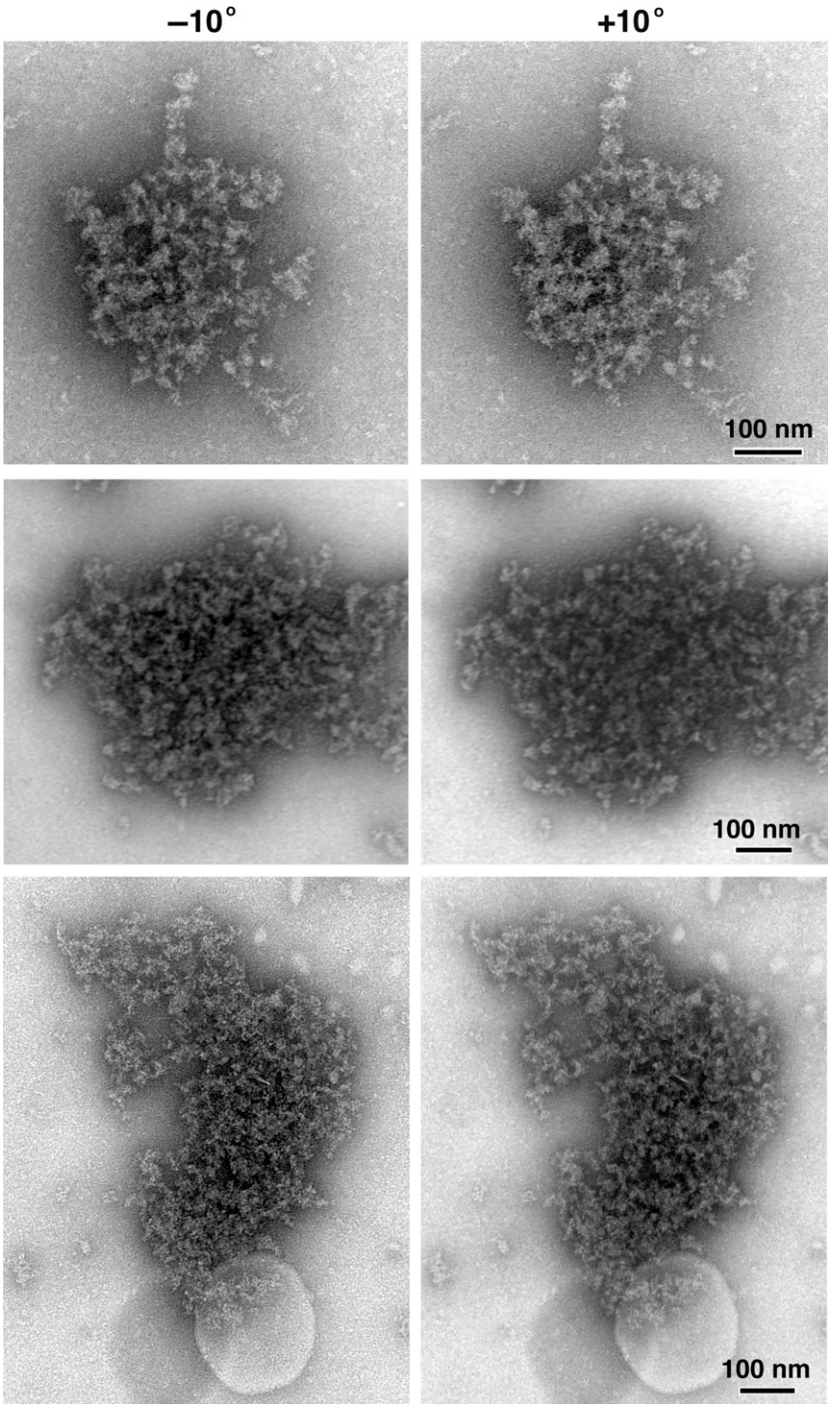

Fig. 2 Stereo view electron microscopy of negatively stained structures contained in the 1% n-Octyl-β-D-glucoside (OG)-IS-11B. Typical three examples are shown. Stage was tilted −10° and +10°, respectively, from the horizontal position.

lattice', which was prepared by treatment of 'regular' TX-PSD (see Methods) with DOC according to the method reported previously (Blomberg *et al.* 1977). Structures similar to those identified in the 1% OG-IS-11B were found in the 'authentic PSD lattice' preparation, and these structures were immuno-labeled with anti-tubulin and anti-β-actin antibodies; the representative EM images are shown in Figure S8. The results suggest that the structures contained in the 1% OG-IS-11B are purified PSD lattice structures.

The amount of typical PSD proteins on the structures in the 1% OG-IS-11B and 1% OG-PSD (1% OG-IS-12 in this case) (Figure S6 and S7) was quantitated and the results are summarized in Fig. 6. Structures of which morphology were apparently different from those shown in Fig. 2 (see

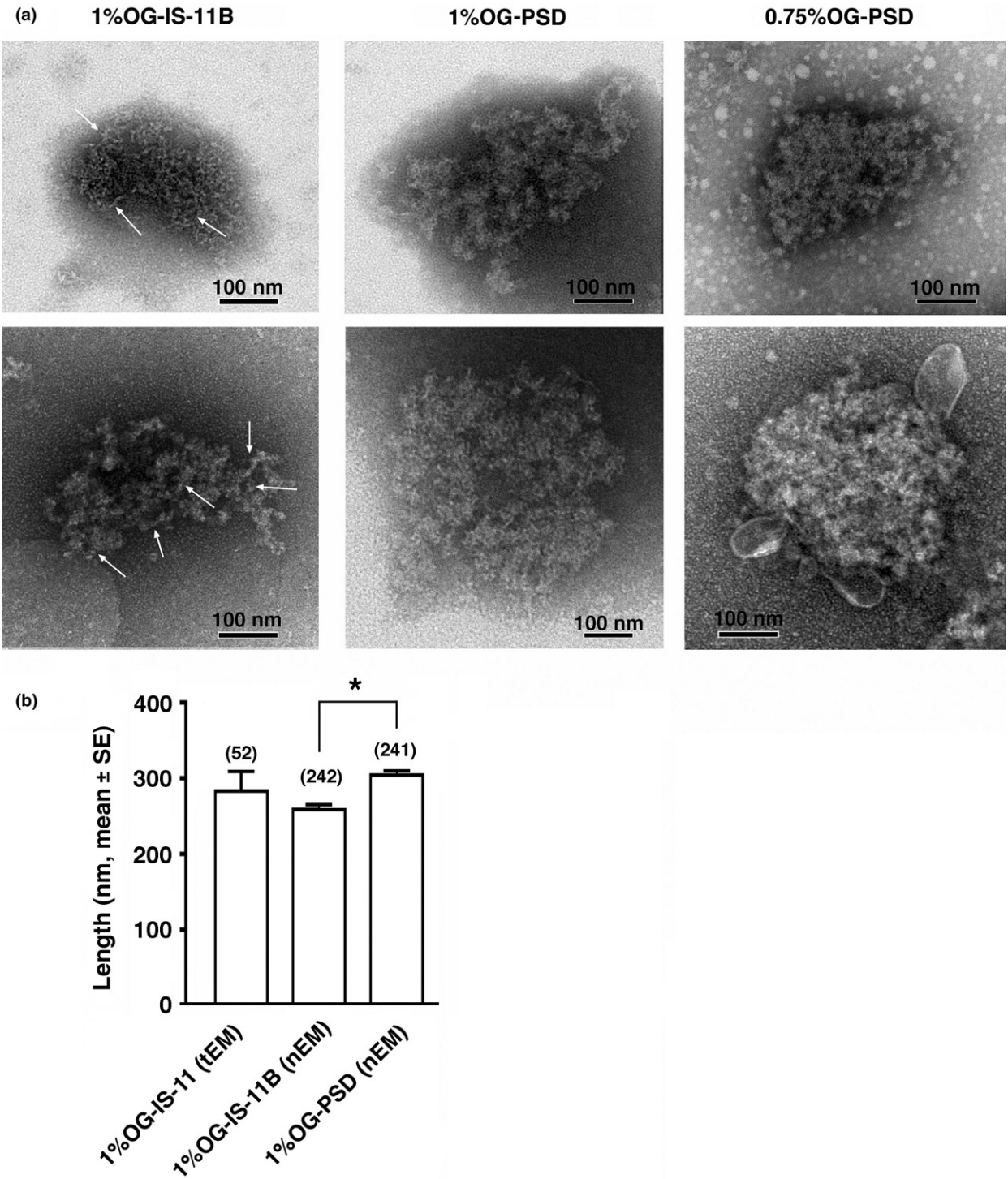

Fig. 3 Comparison of the structures in the 1% n-Octyl-β-D-glucoside (OG)-IS-11B with those in OG-post-synaptic density (PSD)s. (a) Negatively stained electron micrographs of structures in 1%OG-IS-11B, 1%OG-PSD, and 0.75%OG-PSD (1%OG-12 and 0.75%OG-12, respectively). Typical two examples are shown. Arrows indicate typical mesh-like structures. Scales, 100 nm. (b) Longest diameter of the structure of 1%OG-IS-11, 1%OG-IS-11B, and 1%OG-PSD (1% OG-IS-12). *n*, shown in parentheses. $*p < 0.0001$, Mann–Whitney test. tEM and nEM are thin section EM and negatively stained EM, respectively.

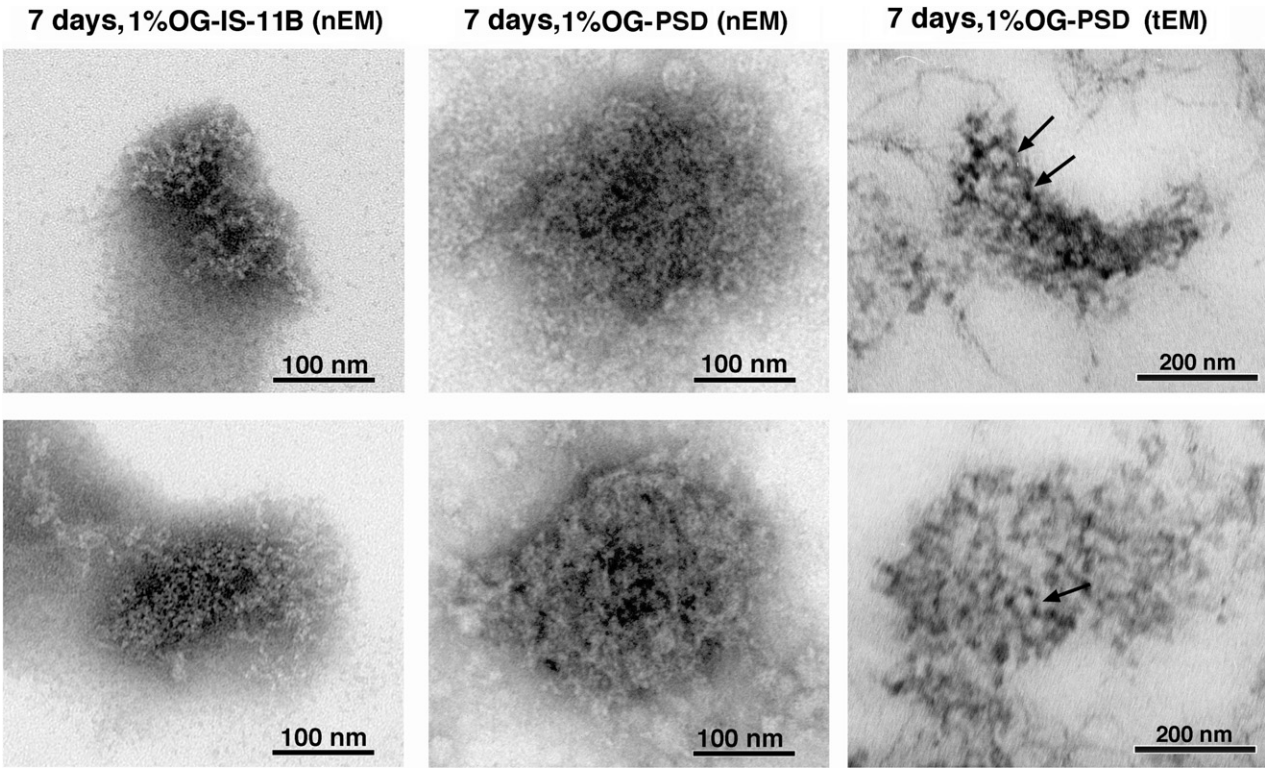

Fig. 4 Presence of post-synaptic density (PSD) lattice-like structure in the % n-Octyl-β-D-glucoside (OG)-IS-11B prepared from immature forebrain. Electron micrographs of structures contained in 1%OG-IS-11B and 1%OG-PSD (1%OG-12 in this case) prepared from 7-day-old rat forebrains. tEM and nEM are thin section EM and negatively stained EM, respectively. Arrows indicate typical mesh-like structures observed in the 7 days-PSDs. Typical examples are shown.

Figure S9) were excluded from counting the immuno-gold particles. Levels of control, in which primary antibodies were omitted, were very low in both 1% OG-IS-11B and 1% OG-PSD. Brief digestion with pepsin (gray bars in Fig. 6) increased the numbers of labels for some PSD proteins, in particular, many PSD scaffold proteins and actin in the PSD, and PSD-95 in 1% OG-IS-11B. This implies that primary antibodies against these proteins were not easily accessible owing to internal localization of the target proteins in the structures or blocking of antigenic sites by nearby associating proteins even though they are localized near the surface. Relatively internal localization in the PSD structure explains this result for many PSD scaffold proteins. The responses to pepsin digestion were not necessarily the same between 1% OG-IS-11B and 1% OG-PSD even in the same proteins. This may be mainly owing to the difference in sparseness of the two structures, and absence of proteins hindering access of antibodies to some target proteins in the 1% OG-IS-11B. Pepsin pre-treatment was required for labeling of PSD-95 in 1% OG-PSD and the requirement was not changed in 1% OG-IS-11B, whereas the requirement was changed in the case of Shank1. Levels of SAP102 and Homer in both 1% OG-PSD and 1% OG-IS-11B were changed as much after pepsin pre-treatment. Thus, the pre-treatment was not required for labeling of SAP102 and Homer. Pepsin pre-treatment was not carried out when labeling the α-IN, CaMKIIα and β, and NF-L on 1% OG-IS-11B, since the pre-treatments were not necessary for these labeling in 1% OG-PSD, which is denser than the 1% OG-IS-11B. Immuno-gold label for GKAP was rarely detected by 10-nm gold and the label did not significantly increase after pepsin digestion for 2 min. Therefore, we used 5-nm gold particles to examine the GKAP distribution in both structures.

Analysis of protein components of immature PSD lattice structure by immuno-gold negative staining EM

Distribution of typical PSD proteins was also examined in the immature 1% OG-IS-11B in a similar way as in the adult structure. Presence of tubulin and β-actin in 7 days, 1% OG-IS-11B was confirmed as shown in Fig. 7(a) and (b). Both tubulin and β-actin were localized in the small structures (e.g., < 100 nm in diameter), possibly nascent fragments or partly broken fragments during detergent treatment of immature SPM. Difference in morphology and size of negatively stained 7 days, 1% OG-IS-11B structures may be because of variability in maturity of the structures.

Contents of typical PSD proteins in the immature structures were quantitated as summarized in Fig. 7(c). In the case

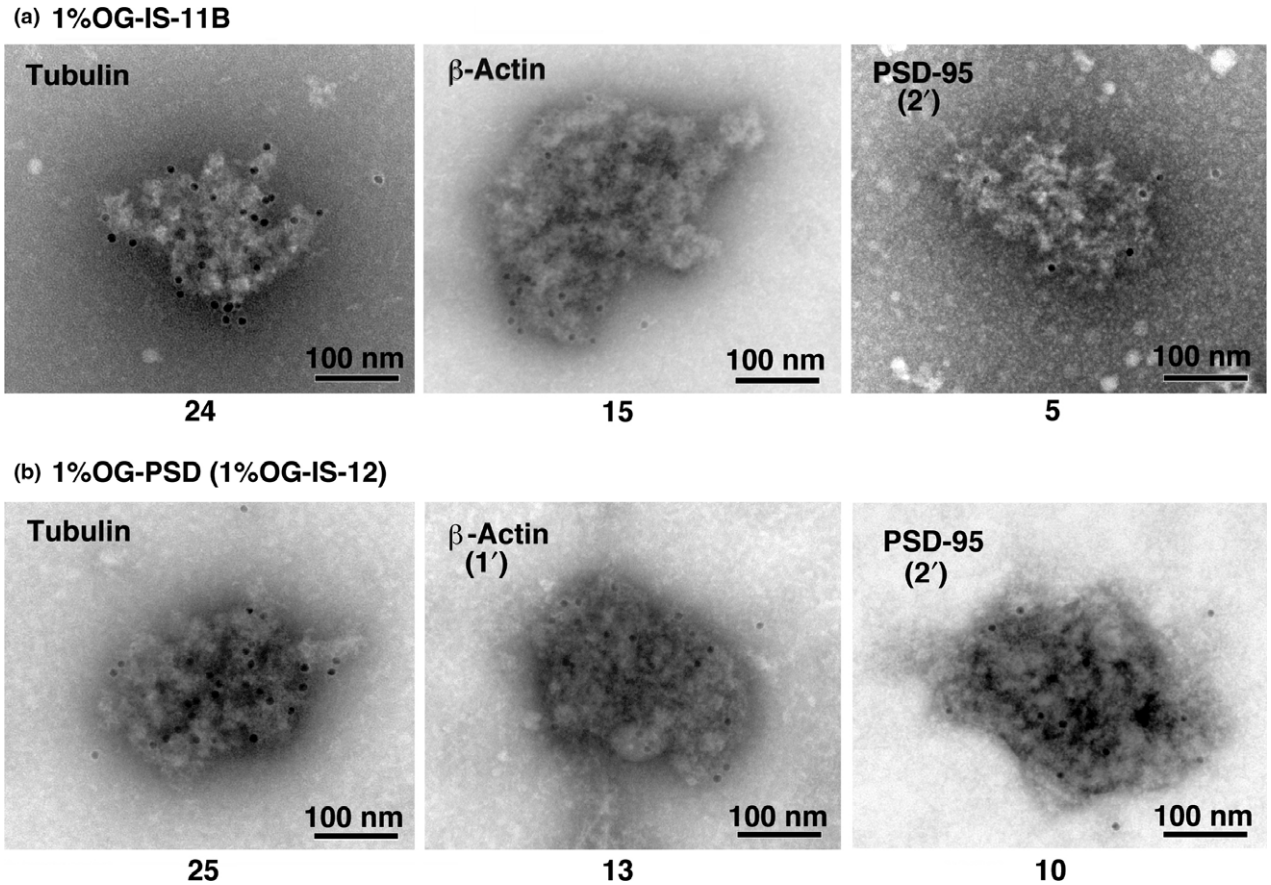

Fig. 5 Immuno-gold electron microscopic observation of post-synaptic density (PSD) proteins in 1% n-Octyl-β-D-glucoside (OG)-IS-11B structure and 1%OG-PSD (1%OG-IS-12). Immuno-gold negative staining was applied to detect distribution of typical cytoskeletal and scaffold proteins in PSDs. Structures in the 1%OG-IS-11B or 1% OG-IS-12 were spotted on formvar membrane on the EM grid, labeled with antibodies listed in Table 2, followed by gold-labeled antibody, and negatively stained with nano-W. Typical examples for tubulin, β-actin, and PSD-95 are shown. See Figures S6 and S7 for the other PSD proteins. Sizes of immuno-gold particle are 10 nm. The durations of pepsin treatment are indicated in the parentheses below the protein names. Samples without these indications were not treated with pepsin. Scales, 100 nm. The number of gold particles are indicated below each photograph.

of immature 1% OG-IS-11B, pepsin digestion was avoided because it caused severe damage to the structure and made it difficult to identify lattice-like structures. Instead, we used 5-nm immuno-gold particles to label the scaffold proteins and CaMKII. For label of cytoskeletal proteins, 10-nm gold was used since there appeared to be no problem in the access of the 10-nm gold to cytoskeletal proteins judging from the result of the adult 1% OG-IS-11B. We did not examine NF-L because the protein was not present, and very scarce, in the adult 1% OG-IS-11B and 1% OG-PSD, respectively (Fig. 6). Anti-Homer 1 or anti-Homer 3 mouse monoclonal antibodies were used instead of anti-Homer goat polyclonal antibody (sc-8921; Santa Cruz, CA, USA) in this study. Tubulin was the most abundant in immature 1% OG-IS-11B. SAP102 and GKAP were very low in their contents in the immature sample. Tubulin, Shank1, β-actin, α-IN, CaMKIIβ were approximately the same as those in the adult structure: PSD-95 and Homer were approximately 2-fold, CaMKIIα was approximately half (compare Figs 6a and 7c). Low content of CaMKIIα in the 7-day-old sample is in parallel to its low expression in the early developmental days (Kelly *et al.* 1987).

Analyses of protein components of PSD lattice by western blotting and immuno-dot blot assays

Protein components were analyzed by SDS–PAGE to confirm the protein composition of the PSD lattice (1% OG-IS-11B) (Fig. 8a). Both 1% OG-IS-11 and 1% OG-IS-11B were highly enriched with actin (Fig. 8a, Figure S2), which was identified through mass spectrometry and western blotting. Thus, actin was substantially a mere or a major component of 1% OG-IS-11 and 1% OG-IS-11B, according to SDS–PAGE. This result contrasts the results by immuno-gold EM examination.

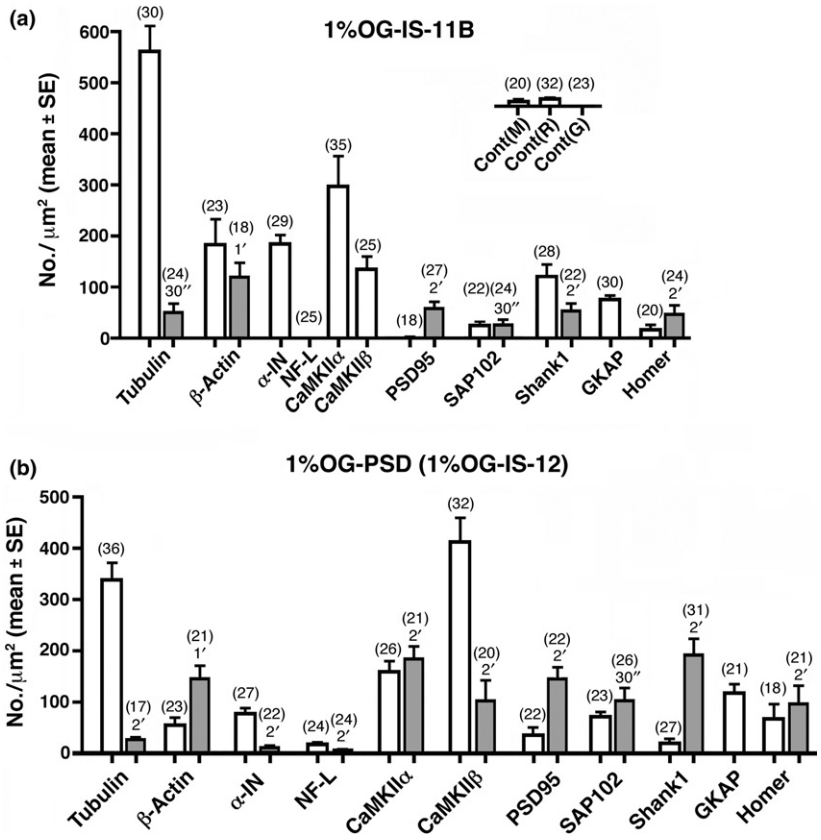

Fig. 6 Quantitative analyses of various post-synaptic density (PSD) proteins in the 1% n-Octyl-β-D-glucoside (OG)-IS-11B and 1%OG-IS-12 structures. Immuno-gold labeling of various kinds of PSD protein to 1%OG-IS-11B structure (a) and OG-PSD (1%OG-IS-12 in this case) (b) were counted and numbers of gold particles per 1 μm^2 were plotted. Gray and white bars are plots of samples with or without pre-treatment with pepsin. Numbers above gray bar are time periods of pepsin digestion (minutes or seconds). Sample numbers are indicated in the parenthesis above each bar. Numbers in controls (Cont) using 2nd antibodies against mouse (M), rabbit (R), or goat (G) IgG without using primary antibodies are also plotted on the top right in (a). Controls in the 1%OS-IS-12 were at the same levels as in (a).

To further analyze the protein components, contents of typical PSD cytoskeletal proteins and scaffold proteins in the 1% OG-IS-11, 1% OG-IS-11B, and 1% OG-IS-12 were examined through western blotting (Fig. 8b). First, the contents of tubulin and α-IN were unexpectedly found to be extremely low compared with 1% OG-IS-12 in western blotting. This result was different from those obtained from immuno-gold negative staining, in which tubulin was highly enriched in both the PSD lattice and the PSD (Fig. 6). There was no band immunoreactive to PSD-95 in 1% OG-IS-11 and 1% OG-IS-11B, and no GKAP-immunoreactive band in all three preparations. Homer1, CaMKII, and β-actin were detected in the 1% OG-IS-11B. CaMKIIβ, but not CaMKIIα, appeared to be concentrated in the 1% OG-IS-11B. β-actin was greatly concentrated in both 1% OG-IS-11 and 1% OG-IS-11B.

To investigate the reason for the discrepancy between western blotting and immuno-gold negative staining, we carried out the immuno-dot blot assay. Representative dot blot images for each protein were aligned with the western blot membrane for comparison (Fig. 8b). Profiles of protein distribution in the three preparations, revealed by immuno-dot blot assay, were substantially the same as those obtained from western blotting for PSD-95, Homer1, CaMKIIβ, and β-actin. In contrast, the profiles were different between western blotting and immuno-dot blot assay for GKAP, α-IN, tubulin, and CaMKIIα. Thus, western blot analysis and immuno-dot blot assay yielded different distribution profiles of proteins on these three preparations.

Pre-treatment of the protein-blotted membrane with pepsin, as was done in immuno-gold EM, lowered protein contents held on the membrane and deterred the immunological detection of the protein. The presence of tubulin and α-IN in the 1% OG-IS-11B was confirmed by preliminary proteomic analyses (not shown).

In summary, proteins contained in the IS-11B were solubilized with SDS-mercaptoethanol to variable extents: some proteins, such as tubulin and α-IN, were extremely insoluble to SDS and mercaptoethanol (Fig. 8). Next, we examined the 1% OG-IS-11B by negative staining EM after boiling them for 3 min in the presence of SDS-mercaptoethanol (2.1% and 3.6%, respectively) and found PSD lattice-like structures which contained tubulin and α-IN (Figure S10).

Discussion

PSD lattice structure was purified

We investigated novel structures contained in a, as yet unknown, fraction derived from SPM. The structures contained in the fraction are similar to PSDs in terms of

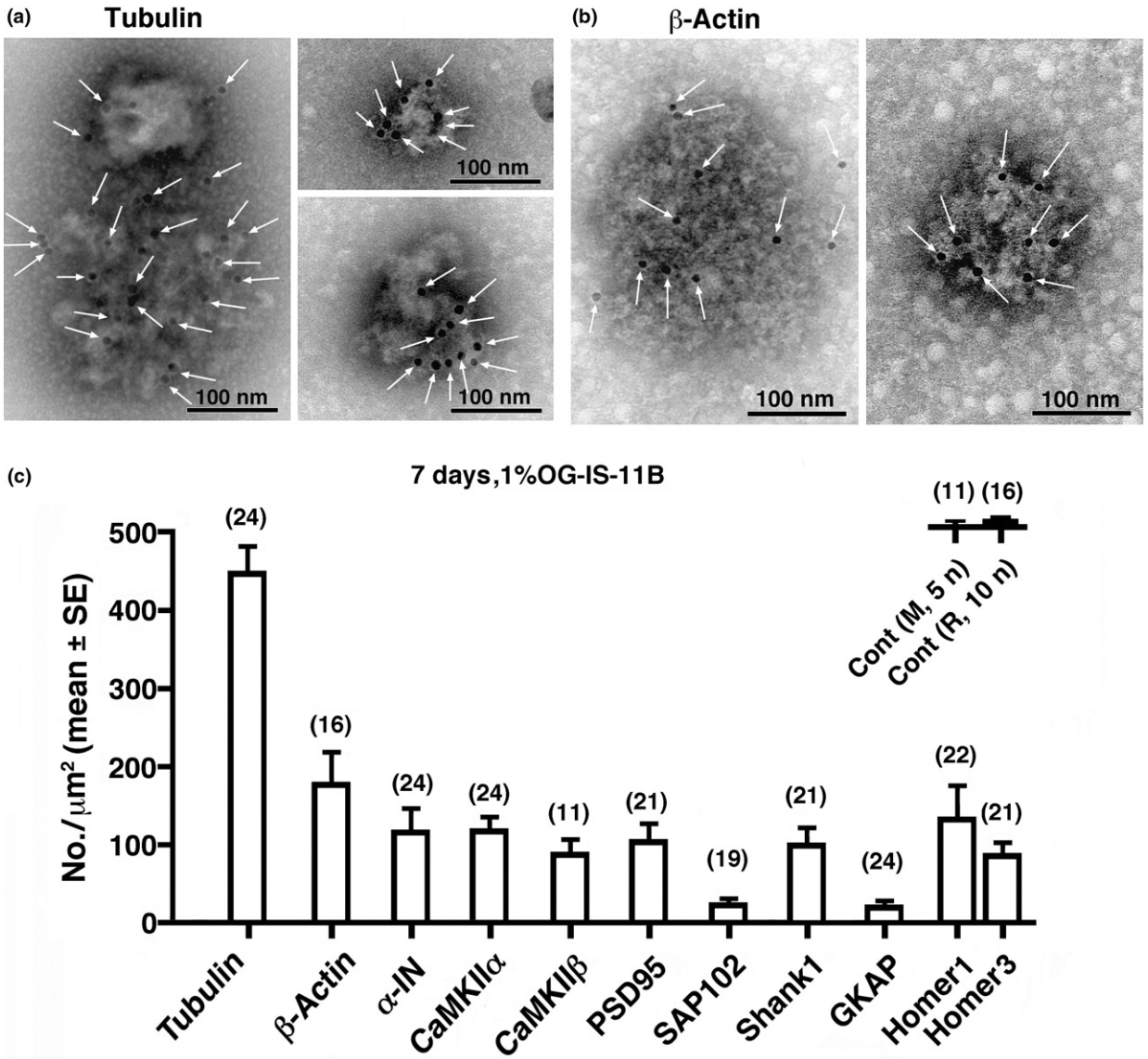

Fig. 7 Immuno-gold electron microscopic observation of various post-synaptic density (PSD) proteins in immature 1% n-Octyl-β-D-glucoside (OG)-IS-11B structure. (a and b) Immuno-gold negative staining was carried out for 7 days, 1%OG-IS-11B structures. Typical examples for tubulin (a) and β-actin (b) are shown. Control experiment without using primary antibody showed substantially no label on the structures (not shown). Arrows indicate gold particles. (c) Quantitative analyses of various PSD proteins in the 7 days, 1%OG-IS-11B structures. Anti-tubulin and α-IN antibodies are rabbit origin, and 10-nm gold particle was used as well as labeling of β-actin. Five-nm gold particle was used in the other cases. Sample numbers are indicated in the parenthesis above each bar. For controls (Cont), immunolabeling was carried out using 2nd antibodies against mouse (M) or rabbit (R) IgG without using primary antibodies.

size, planar nature, and morphology at EM level in both thin sections and negative staining. The structures appear to be constructed by woven fibrous materials, and make mesh-like frameworks. The structures are sparser and slightly lighter than PSDs. They contained typical PSD scaffold proteins, although their contents were lower than the PSD (Fig. 6). Furthermore, the structure appears to be the same as the DOC-insoluble 'authentic PSD lattice' (Matus and Walters 1975; Matus and Taff-Jones 1978; Matus 1981). These results suggest that the structures concentrated in the 1% OG-IS-11B are related to PSD and they are PSD lattice structures. The presence of the mesh-like structure is supported by the disclosure of such structure by harsh solubilization of PSDs (ex. with 5% TX-100) (Guo *et al.* 2017). A similar structure, interlaced fiber network structure of PSD, is clearly shown in the synaptic complex prepared using p-iodonitrotetrazlium, a protein cross-linker (Suzuki *et al.* 2008), and further treated with 1 or 8 M urea and

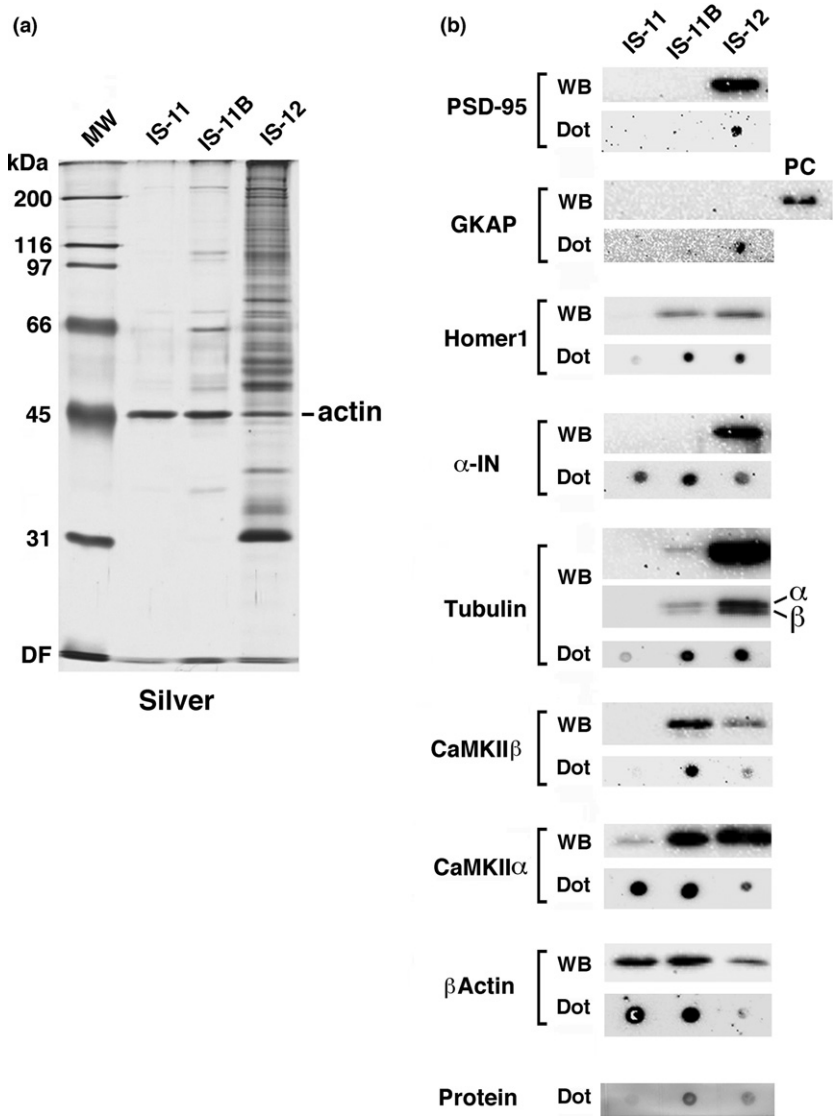

Fig. 8 Protein analyses by sodium dodecyl sulfate–polyacrylamide gel electrophoresis, western blotting, and dot blotting. (a) Comparison of protein profiles of 1% n-Octyl-β-D-glucoside (OG)-IS-11, 1%OG-IS-11B, and 1%OG-IS-12. These fractions were simultaneously prepared from synaptic plasma membrane and the same volume of each sample was applied to each lane and proteins stained with silver were compared. Actin was identified by western blotting and mass spectrometry. (b) Comparison of various PSD proteins by western blotting (WB) and immuno-dot blotting (Dot). The same volume of fractions (4 and 2 μL for western and immuno-dot, respectively) was applied. The same antibodies as those used for immuno-gold negative staining were used to avoid complexity in evaluation of the results. Four sets of different preparations were examined and representative results are shown. Lane marked by PC is a positive control for GKAP western blotting using 1% OG-12. Dot blot of total proteins contained in each fraction stained with SYPRO Ruby is also shown at the bottom. Lower image of western blotting of tubulin shows the presence of both α and β subunits. '1% OG' in fraction names is omitted in the figure for simplicity.

mild sonication (Cotman and Taylor 1972). Thus, the mesh-like structure appears to be a backbone structure of the PSD, which is buried underneath the PSD. Mesh-like structures similar to the PSD lattice were also indicated in the platinum-shadowed adult PSDs (Petersen *et al.* 2003). Therefore, the meshwork structure does not appear to be an artifact produced after treatment of synapses with detergents. Thus, this experiment supports the idea that the mesh-like structure is present underneath the PSD and that it is a backbone structure of PSD. The purified structure may be different from actin meshworks which expand from PSD into a whole cytoplasm of spine (Gulley and Reese 1981; Cohen *et al.* 1985).

Protein components of purified PSD lattice

Protein components of the PSD lattice were validated by immuno-gold labeling EM, since western blotting was not reliable owing to insolubility of some components of the PSD lattice to SDS-mercaptoethanol (Fig. 8b). Tubulin was the most abundant component among those tested, based on the immuno-gold EM analysis (Fig. 6). Actin, α-IN, and CaMKII were also relatively abundant compared with typical PSD scaffold proteins. Tubulin was also abundant in the adult type I PSD compared with the typical PSD scaffold proteins. Actin content is in the same level among the PSD lattice and the PSD, and α-IN is slightly less abundant than typical scaffold proteins in the adult type I PSD. Another typical cytoskeletal protein, NF-L, was very sparse in both the PSD lattice and PSD of type I synapse. Typical PSD scaffold proteins were present in the isolated PSD lattice, however, their contents were lower than those in PSD. Thus, tubulin, actin, α-IN, and CaMKII are abundant protein constituents of the adult PSD lattice. Effects of pepsin digestion differed between the PSD lattice and PSD, which

suggests a difference in the accessibility of antibody to each protein in these structures.

In the immature PSD lattice prepared from 7-day-old rats, tubulin was the most abundant protein, whereas actin, α-IN, and CaMKII were in the same level with some of PSD scaffold proteins (Fig. 7). Extremely low abundance of SAP102 and GKAP in the immature PSD lattice, suggests that both proteins are not involved in the initial formation of PSD lattice of type I synapses. In particular, SAP102 was less abundant than PSD-95 in the PSD lattice, even in the early developmental days when its expression was higher than adult days in the PSD (Sans *et al.* 2000; Petralia *et al.* 2005; Zheng *et al.* 2011). The result suggests that SAP102 is not involved in formation and maintenance of the PSD lattice of type I synapses, and is in good agreement with a report that SAP102 is primarily responsible for synaptic trafficking of α-amino-3-hydroxy-5-methylisoxazole-4-propionate and NMDA receptors during synaptogenesis (Elias *et al.* 2008). GKAP may be incorporated into PSD and PSD lattice structures in later developmental stages. Relative abundance of some PSD scaffold proteins, such as PSD-95, Shank1, and Homer, suggest association of such MAGUK proteins with immature PSD lattice.

Our results thus suggest that the PSD lattice, of both adult and 7-day-old rats, is constructed with both major cytoskeletal proteins and PSD scaffold proteins among which, one of the major components is tubulin. Although, it is not yet clearly known whether cytoskeletal proteins alone, without PSD scaffold proteins, can organize a PSD lattice, the tubulin-based PSD lattice is formed in the early stage of synaptogenesis and then other PSD proteins, such as scaffold proteins, become associated with the lattice as PSD matures. We propose that a tubulin-containing structure forms the PSD lattice, the backbone framework for the PSD structure.

SDS-insolubility of tubulin and α-IN were observed in the PSD lattice prepared in this study. Such SDS-insoluble property of tubulin has also been demonstrated in the previous report (Li *et al.* 2004). We are now intensively investigating on this matter.

Tubulin, actin, α-IN, and CaMKII in the PSD

There are accumulating EM data using diaminobenzidine suggesting the presence of tubulin in the PSD (Matus *et al.* 1975; Caceres *et al.* 1984). High labeling of PSD not expanding to the cytoplasmic area of outside PSD (Caceres *et al.* 1984) suggests that tubulin is confined to the PSD. It has been suggested that tubulin is present in the PSD in non-microtubule form (Matus *et al.* 1975).

It is well established that actin is a major cytoskeletal components in dendritic spines of neuronal cells (Capani *et al.* 2001b). Number of studies using various EM techniques wide distribution of actin in the PSD along the depth from post-synaptic membrane to the cytoplasmic surface of the PSD pallium (Matus *et al.* 1982; Caceres *et al.* 1983; Cohen *et al.* 1985; Capani *et al.* 2001a,b; Rostaing *et al.* 2006). Analysis of PSD using the Nano-Depth-Tagging method suggested that actin resides inside of the PSD (Yun-Hong *et al.* 2011).

There are only a few studies regarding α-IN, 66-kDa neurofilament subunit, in the PSDs. Immuno-EM study using diaminobenzidine (Suzuki *et al.* 1997) reported the relatively confined distribution of α-IN to PSD, and the distribution of α-IN in PSD starts before the period of synaptogenesis.

CaMKII is localized in both the core and cytoplasmic surface of the PSD by negative staining EM tomography (Fera *et al.* 2012). Nano-Depth-Tagging method also supports localization of the enzyme inside the PSD (Liu *et al.* 2006; Chang *et al.* 2007; Yun-Hong *et al.* 2011).

Thus, these reports support our finding that these cytoskeletal proteins are associated with the PSD lattice. However, it should be clarified whether tubulin in the PSD lattice is not postmortem accumulation, since microtubules at the post-synaptic region depolymerize easily by cooling (Kirov *et al.* 2004) and tubulin accumulates to the PSD postmortem (Carlin *et al.* 1982).

Relationship between the PSD lattice structure and the PSD scaffold assemblies

The PSD consists of two classes of structural units: scaffold-assembled receptor complex (e.g., PSD-95 complex) and PSD lattice. Our results suggest that the PSD lattice structure is not a construct built only or mainly by PSD scaffold proteins, rather mainly by tubulin, actin, α-IN, and CaMKII. We propose here a 'combined scaffold-organized components and PSD lattice' model for PSD molecular architecture (Fig. 9): PSD lattice may form a basic framework underlying the PSD structure and may affect the overall synaptic structure. Tubulin, actin, and α-IN may be essential components for the PSD lattice, and scaffold proteins alone may not be able to form this basic framework structure. Scaffold proteins at synapses have two major roles: roles for structure and for signaling complex formation and linkage (Won *et al.* 2017). MAGUKs, one type of scaffold proteins, may play a greater role in the formation of functional protein complexes or nanodomains/nanocolumns in the PSD, than a direct structural role for PSDs.

One experiment reported the existence of type I PSDs that lacked either one of PSD-95, PSD-93, SAP97, or SAP102 proteins, although we do not know whether such PSD lacks all of PSD-95 family MAGUK proteins (Aoki *et al.* 2001). The content of PSD-95 in PSDs was variable. Farley *et al.* (2015) reported that PSD-95 is the most abundant scaffold in cortical PSDs but not in hippocampal and cerebellar PSDs, and PSD-95 was absent in one type of cerebellar PSD. Recently, triple knockdown of three typical MAGUK proteins, PSD-95/Dlg4, PSD-93/chapsin110/Dlg2, and SAP102/Dlg3, demonstrated that MAGUK proteins have a central role in maintaining and anchoring GluRs at the PSD but not in the formation of overall synapse structures including positioning of pre-and post-synaptic membranes

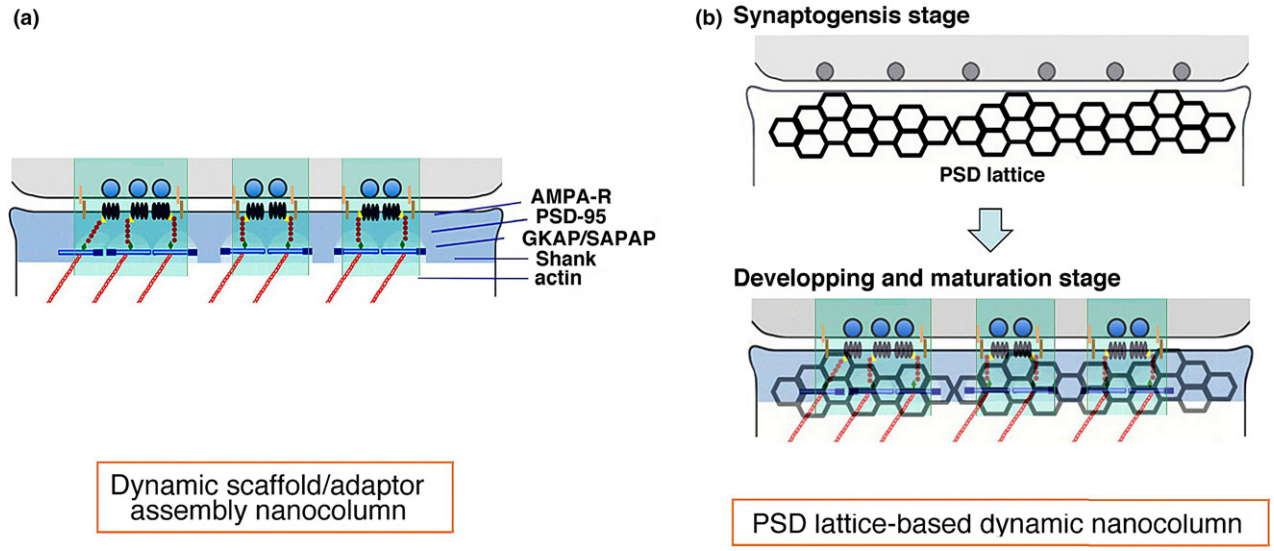

Fig. 9 Models for protein architecture post-synaptic density (PSD)s. (a) 'Dynamic scaffold/adaptor assembly nanocolumn' model modified from (Tang *et al.* 2016), where pre-synaptic and post-synaptic structures make column-like structures perpendicular to the synaptic membrane. Post-synaptic portion of the column was constructed from PSD scaffold assembly. Organization and distribution of the column in the synaptic area are dynamic in nature. (b) 'PSD lattice-based dynamic nanocolumn' model, a new PSD organization model based on this study. PSD lattice structure which is mainly constructed with tubulin and α-IN is constructed early in synaptogenesis and works as a basic structure of the PSD. PSD scaffold proteins become associated with the PSD lattice structure and make a nanocolumn protein complex. Association and organization of the nanocolumn structure with PSD lattice change dynamically during development and upon synaptic stimulation.

(Chen *et al.* 2015), because pre- and post-synaptic membranes remained normal even though electron-dense structures corresponding to 'PSD core' (Dosemeci *et al.* 2016) and both α-amino-3-hydroxy-5-methylisoxazole-4-propionates and NMDARs, were reduced at the PSD. The triple knockdown produced the presence of synapses without highly electron-dense PSD structures, which were regarded as immature synapses (Chen *et al.* 2015). If they are immature synapses, they lack PSD-95 or other MAGUK proteins. Thus, the role of MAGUKs are rather related to the appearance of the highly electron-dense 'PSD core' layer and do not cover the overall region of the PSD (PSD plus PSD pallium) or overall synaptic structure. PSD-95 may not be involved in the formation of initial synaptic sites because synaptic vesicle accumulation at the synapse-forming site preceded PSD-95 accumulation (Okabe *et al.* 2001). In addition, PSD-95 increased in non-synaptic NMDA receptor-island, possibly a nascent PSD, in later stage of development (Tao-Cheng et al., 2015). Thus, overall structures of excitatory synapses do not appear to be formed, nor maintained by MAGUK proteins alone.

However, roles of scaffold proteins other than MAGUKs, in particular, Shank, GKAP, and Homer, may have greater roles for PSD structures, as well as those related to signaling protein complexes and their linkage. They interconnect themselves and general cytoskeletons, and thus participate in the structural role, in particular in the PSD pallium region. Structural roles of scaffold proteins are supported by the facts that over-expression or down-regulation of scaffold proteins, such as Shank, affects the size of the spine (Sala *et al.* 2001). Shank translocated to the PSD pallium (Tao-Cheng *et al.* 2010; Dosemeci *et al.* 2016) may be involved in the enlargement of highly electron-dense regions of PSDs. Shank is responsible for high electron density of PSDs but not for the overall structure of synapse, from the Shank-depleted/reduced experiments (Grabrucker *et al.* 2011). GKAP plays a structural role by connecting the PSD-95 layer and the Shank layer. Shank proteins form a sheet-like structure, which could be a platform for the construction of the PSD complex (Baron *et al.* 2006). Homer and Shank make a polymeric network structure (Hayashi *et al.* 2009), and both proteins appear to coordinately induce spine enlargement (Sala *et al.* 2001).

Our model could be supported by the fact that contents of tubulin, actin, CaMKII, and α-IN, are much higher than those of PSD-95 and other PSD scaffold proteins (Lai *et al.* 1999; Peng *et al.* 2004; Cheng *et al.* 2006). The idea of tubulin-core in our model is supported by the presence of tubulin in the core region of PSD (Ratner and Mahler 1983; Yun-Hong *et al.* 2011). The PSD lattice may be connected to microtubules because the direct connection of microtubules to PSD is observed in both mature and immature brains (Westrum and Gray 1977). Transiently formed microtubules in the spine may be related to PSD maturation and plastic changes.

The PSD lattice becomes visible when associated PSD proteins are greatly extracted from highly electron-dense PSD, e.g. by DOC and 5% TX-100. Therefore, the PSD lattice resides in the electron-dense 'PSD core' region, where PSD-95 resides and GKAP is nearby. Considering that the purified PSD lattice contains Shank and Homer, which are pallium residents, the PSD lattice may include the PSD pallium region. This point should be verified in the future. The PSD lattice does not hold glutamate receptors because our shotgun proteomics analysis detected only 2 glutamate receptor subunit-derived peptides among 2310 peptides detected (not shown).

Conclusions

We purified the PSD lattice structure, which is constructed majorly of tubulin, actin, and α-IN rather than typical PSD scaffold proteins. We propose here a new PSD architecture model, which is a combination of the PSD lattice structure and the PSD scaffold assemblies.

Acknowledgments and conflict of interest disclosure

We acknowledge Dr. Fujii for generously providing anti-tubulin antibody, Dr. K. Nakayama for anti-β-tubulin, and Dr. S. Taniguchi for anti-β-actin antibody. All of these researchers are in Shinshu University. This work was supported by Distinguished Visiting Professor system of Interdisciplinary Cluster for Cutting Edge Research, Shinshu University (to W.L.) and funded by a Grant from Institute for Biomedical Sciences, Interdisciplinary Cluster for Cutting Edge Research Shinshu University, and from School of Medicine, Shinshu University Academic Assembly (both to T.S.). We would like to thank Editage (www.editage.jp) for English language editing. The authors have no conflict of interest to declare.

All experiments were conducted in compliance with the ARRIVE guidelines.

Supporting information

Additional Supporting Information may be found online in the supporting information tab for this article:

Figure S1. Purification of PSD lattice (1% OG-IS-11B) and other detergent-insoluble fractions from SPM.

Figure S2. SDG analysis of SPM after solubilization with 1% OG.

Figure S3. Three-dimensional view of isolated 1% OG-IS-11 structure viewed by EM tomography. (Video S1 and Video S2)

Figure S4. Structure contained in the OG-PSD.

Figure S5. Stereo view electron microscopy of negatively stained structures contained in 7 days, 1% OG-IS-11B.

Figure S6. Immuno-gold electron microscopic observation of various PSD proteins in 1% OG-IS-11B structure.

Figure S7. Immuno-gold electron microscopic observation of various PSD proteins in 1% OG-PSD (1% OG-IS-12).

Figure S8. Presence of tubulin and actin on the "authentic PSD lattice".

Figure S9. Heterogeneity of PSD-like structures found in the 1% OG-IS-11B.

Figure S10. Immuno-gold microscopic observation in SDS-insoluble structure.

References

Aoki C., Miko I., Oviedo H., Mikeladze-Dvali T., Alexandre L., Sweeney N. and Bredt D. S. (2001) Electron microscopic immunocytochemical detection of PSD-95, PSD-93, SAP-102, and SAP-97 at postsynaptic, presynaptic, and nonsynaptic sites of adult and neonatal rat visual cortex. *Synapse* **40**, 239–257.

Baron M. K., Boeckers T. M., Vaida B., Faham S., Gingery M., Sawaya M. R., Salyer D., Gundelfinger E. D. and Bowie J. U. (2006) An architectural framework that may lie at the core of the postsynaptic density. *Science* **311**, 531–535.

Blomberg F., Cohen R. S. and Siekevitz P. (1977) The structure of postsynaptic densities isolated from dog cerebral cortex. II. Characterization and arrangement of some of the major proteins within the structure. *J. Cell Biol.* **74**, 204–225.

Boeckers T. M. (2006) The postsynaptic density. *Cell Tissue Res.* **326**, 409–422.

Bosch M., Castro J., Saneyoshi T., Matsuno H., Sur M. and Hayashi Y. (2014) Structural and molecular remodeling of dendritic spine substructures during long-term potentiation. *Neuron* **82**, 444–459.

Caceres A., Payne M. R., Binder L. I. and Steward O. (1983) Immunocytochemical localization of actin and microtubule-associated protein MAP2 in dendritic spines. *Proc. Natl Acad. Sci. USA* **80**, 1738–1742.

Caceres A., Binder L. I., Payne M. R., Bender P., Rebhun L. and Steward O. (1984) Differential subcellular localization of tubulin and the microtubule-associated protein MAP2 in brain tissue as revealed by immunocytochemistry with monoclonal hybridoma antibodies. *J. Neurosci.* **4**, 394–410.

Capani F., Deerinck T. J., Ellisman M. H., Bushong E., Bobik M. and Martone M. E. (2001a) Phalloidin-Eosin followed by photo-oxidation: a novel method for localizing F-actin at the light and electron microscopic levels. *J. Histochem. Cytochem.* **49**, 1351–1361.

Capani F., Martone M. E., Deerinck T. J. and Ellisman M. H. (2001b) Selective localization of high concentrations of F-actin in subpopulations of dendritic spines in rat central nervous system: a three-dimensional electron microscopic study. *J. Comp. Neurol.* **435**, 156–170.

Carlin R. K., Grab D. J. and Siekevitz P. (1982) Postmortem accumulation of tubulin in postsynaptic density preparations. *J. Neurochem.* **38**, 94–100.

Chang C. W., Peng S. C., Cheng W. Y., Liu S. H., Cheng H. H., Huang S. Y. and Chang Y. C. (2007) Studying the protein-protein interactions in the postsynaptic density by means of immunoabsorption and chemical crosslinking. *Proteomics Clin. Appl.* **1**, 1499–1512.

Chen X., Levy J. M., Hou A., Winters C., Azzam R., Sousa A. A., Leapman R. D., Nicoll R. A. and Reese T. S. (2015) PSD-95 family MAGUKs are essential for anchoring AMPA and NMDA receptor complexes at the postsynaptic density. *Proc. Natl Acad. Sci. USA* **112**, E6983–E6992.

Cheng D., Hoogenraad C. C., Rush J. *et al.* (2006) Relative and absolute quantification of postsynaptic density proteome isolated from rat forebrain and cerebellum. *Mol. Cell Proteomics* **5**, 1158–1170.

Cohen R. S., Wolosewick J. J., Becker R. P. and Pappas G. D. (1983) Fine structure of synapses of the central nervous system in resinless sections. *J. Submicrosc. Cytol.* **15**, 849–863.

Cohen R. S., Chung S. K. and Pfaff D. W. (1985) Immunocytochemical localization of actin in dendritic spines of the cerebral cortex using colloidal gold as a probe. *Cell. Mol. Neurobiol.* **5**, 271–284.

Cotman C. W. and Taylor D. (1972) Isolation and structural studies on synaptic complexes from rat brain. *J. Cell Biol.* **55**, 696–711.

DeGiorgis J. A., Galbraith J. A., Dosemeci A., Chen X. and Reese T. S. (2006) Distribution of the scaffolding proteins PSD-95, PSD-93, and SAP97 in isolated PSDs. *Brain Cell Biol.* **35**, 239–250.

Dosemeci A., Weinberg R. J., Reese T. S. and Tao-Cheng J. H. (2016) The postsynaptic density: there is more than meets the eye. *Front. Synaptic Neurosci.* **8**, 23.

Elias G. M., Elias L. A., Apostolides P. F., Kriegstein A. R. and Nicoll R. A. (2008) Differential trafficking of AMPA and NMDA receptors by SAP102 and PSD-95 underlies synapse development. *Proc. Natl Acad. Sci. USA* **105**, 20953–20958.

Farley M. M., Swulius M. T. and Waxham M. N. (2015) Electron tomographic structure and protein composition of isolated rat cerebellar, hippocampal and cortical postsynaptic densities. *Neuroscience* **304**, 286–301.

Feng W. and Zhang M. (2009) Organization and dynamics of PDZ-domain-related supramodules in the postsynaptic density. *Nat. Rev. Neurosci.* **10**, 87–99.

Fera A., Dosemeci A., Sousa A. A., Yang C., Leapman R. D. and Reese T. S. (2012) Direct visualization of CaMKII at postsynaptic densities by electron microscopy tomography. *J. Comp. Neurol.* **520**, 4218–4225.

Grabrucker A. M., Knight M. J., Proepper C. *et al.* (2011) Concerted action of zinc and ProSAP/Shank in synaptogenesis and synapse maturation. *EMBO J.* **30**, 569–581.

Gulley R. L. and Reese T. S. (1981) Cytoskeletal organization at the postsynaptic complex. *J. Cell Biol.* **91**, 298–302.

Guo W., Liu Q. and Suzuki T. (2017) Protein components of the backbone structure of postsynaptic density of type I excitatory synapses. *Shinshu Med. J.* **65**, 211–224.

Hayashi M. K., Tang C., Verpelli C., Narayanan R., Stearns M. H., Xu R. M., Li H., Sala C. and Hayashi Y. (2009) The postsynaptic density proteins Homer and Shank form a polymeric network structure. *Cell* **137**, 159–171.

Hirokawa N. (1989) The arrangement of actin filaments in the postsynaptic cytoplasm of the cerebellar cortex revealed by quick-freeze deep-etch electron microscopy. *Neurosci. Res.* **6**, 269–275.

Kelly P. T., Shields S., Conway K., Yip R. and Burgin K. (1987) Developmental changes in calmodulin-kinase II activity at brain synaptic junctions: alterations in holoenzyme composition. *J. Neurochem.* **49**, 1927–1940.

Kim E. and Sheng M. (2004) PDZ domain proteins of synapses. *Nat. Rev. Neurosci.* **5**, 771–781.

Kirov S. A., Petrak L. J., Fiala J. C. and Harris K. M. (2004) Dendritic spines disappear with chilling but proliferate excessively upon rewarming of mature hippocampus. *Neuroscience* **127**, 69–80.

Lai S. L., Chiang S. F., Chen I. T., Chow W. Y. and Chang Y. C. (1999) Interprotein disulfide bonds formed during isolation process tighten the structure of the postsynaptic density. *J. Neurochem.* **73**, 2130–2138.

Landis D. M. and Reese T. S. (1983) Cytoplasmic organization in cerebellar dendritic spines. *J. Cell Biol.* **97**, 1169–1178.

Li N., Shaw A. R., Zhang N., Mak A. and Li L. (2004) Lipid raft proteomics: analysis of in-solution digest of sodium dodecyl sulfate-solubilized lipid raft proteins by liquid chromatography-matrix-assisted laser desorption/ionization tandem mass spectrometry. *Proteomics* **4**, 3156–3166.

Liu S. H., Cheng H. H., Huang S. Y., Yiu P. C. and Chang Y. C. (2006) Studying the protein organization of the postsynaptic density by a novel solid phase- and chemical cross-linking-based technology. *Mol. Cell Proteomics* **5**, 1019–1032.

Matus A. (1981) The postsynaptic density. *Trends Neurosci.* **4**, 51–53.

Matus A. I. and Taff-Jones D. H. (1978) Morphology and molecular composition of isolated postsynaptic junctional structures. *Proc. R. Soc. Lond. B Biol. Sci.* **203**, 135–151.

Matus A. I. and Walters B. B. (1975) Ultrastructure of the synaptic junctional lattice isolated from mammalian brain. *J. Neurocytol.* **4**, 369–375.

Matus A. I., Walters B. B. and Mughal S. (1975) Immunohistochemical demonstration of tubulin associated with microtubules and synaptic junctions in mammalian brain. *J. Neurocytol.* **4**, 733–744.

Matus A., Ackermann M., Pehling G., Byers H. R. and Fujiwara K. (1982) High actin concentrations in brain dendritic spines and postsynaptic densities. *Proc. Natl Acad. Sci. USA* **79**, 7590–7594.

Okabe S., Miwa A. and Okado H. (2001) Spine formation and correlated assembly of presynaptic and postsynaptic molecules. *J. Neurosci.* **21**, 6105–6114.

Peng J., Kim M. J., Cheng D., Duong D. M., Gygi S. P. and Sheng M. (2004) Semiquantitative proteomic analysis of rat forebrain postsynaptic density fractions by mass spectrometry. *J. Biol. Chem.* **279**, 21003–21011.

Petersen J. D., Chen X., Vinade L., Dosemeci A., Lisman J. E. and Reese T. S. (2003) Distribution of postsynaptic density (PSD)-95 and Ca2 + /calmodulin-dependent protein kinase II at the PSD. *J. Neurosci.* **23**, 11270–11278.

Petralia R. S., Sans N., Wang Y. X. and Wenthold R. J. (2005) Ontogeny of postsynaptic density proteins at glutamatergic synapses. *Mol. Cell Neurosci.* **29**, 436–452.

Ratner N. and Mahler H. R. (1983) Structural organization of filamentous proteins in postsynaptic density. *Biochemistry* **22**, 2446–2453.

Rostaing P., Real E., Siksou L. *et al.* (2006) Analysis of synaptic ultrastructure without fixative using high-pressure freezing and tomography. *Eur. J. Neurosci.* **24**, 3463–3474.

Sala C., Piech V., Wilson N. R., Passafaro M., Liu G. and Sheng M. (2001) Regulation of dendritic spine morphology and synaptic function by Shank and Homer. *Neuron* **31**, 115–130.

Sans N., Petralia R. S., Wang Y. X., Blahos J. 2nd, Hell J. W. and Wenthold R. J. (2000) A developmental change in NMDA receptor-associated proteins at hippocampal synapses. *J. Neurosci.* **20**, 1260–1271.

Suzuki T. (2011) Isolation of synapse-subdomains by subcellular fractionation using sucrose density gradient centrifugation, in *Neuroproteomics "Springer Protocols Neuromethods*, Vol. **57** (Li K. W. ed.), pp. 47–61. Humana Press, New York.

Suzuki T., Mitake S., Okumura-Noji K., Shimizu H., Tada T. and Fujii T. (1997) Excitable membranes and synaptic transmission: postsynaptic mechanisms. Localization of alpha-internexin in the postsynaptic density of the rat brain. *Brain Res.* **765**, 74–80.

Suzuki T., Du F., Tian Q. B., Zhang J. and Endo S. (2008) Ca2 + / calmodulin-dependent protein kinase IIalpha clusters are associated with stable lipid rafts and their formation traps PSD-95. *J. Neurochem.* **104**, 596–610.

Suzuki T., Zhang J., Miyazawa S., Liu Q., Farzan M. R. and Yao W. D. (2011) Association of membrane rafts and postsynaptic density: proteomics, biochemical, and ultrastructural analyses. *J. Neurochem.* **119**, 64–77.

Swulius M. T., Farley M. M., Bryant M. A. and Waxham M. N. (2012) Electron cryotomography of postsynaptic densities during development reveals a mechanism of assembly. *Neuroscience* **212**, 19–29.

Tang A.-H., Chen H., Li T. P., Metzbower S. R., MacGillavry H. D. and Blanpied T. A. (2016) A trans-synaptic nanocolumn aligns neurotransmitter release to receptors. *Nature* **536**, 210–214.

Tao-Cheng J. H., Dosemeci A., Gallant P. E., Smith C. and Reese T. (2010) Activity induced changes in the distribution of Shanks at hippocampal synapses. *Neuroscience* **168**, 11–17.

Tao-Cheng J. H., et al., (2015) Depolarization of Hippocampal Neurons Induces Formation of Nonsynaptic NMDA Receptor Islands Resembling Nascent Postsynaptic Densities. eNeuro, **2**(6).

Westrum L. E. and Gray E. G. (1977) Microtubules associated with postsynaptic 'thickenings'. *J. Neurocytol.* **6**, 505–518.

Won S., Levy J. M., Nicoll R. A. and Roche K. W. (2017) MAGUKs: multifaceted synaptic organizers. *Curr. Opin. Neurobiol.* **43**, 94–101.

Yun-Hong Y., Chih-Fan C., Chia-Wei C. and Yen-Chung C. (2011) A study of the spatial protein organization of the postsynaptic density isolated from porcine cerebral cortex and cerebellum. *Mol. Cell Proteomics* **10**, M110.007138.

Zhao L., Sakagami H. and Suzuki T. (2014) Detergent-dependent separation of postsynaptic density, membrane rafts and other subsynaptic structures from the synaptic plasma membrane of rat forebrain. *J. Neurochem.* **131**, 147–162.

Zheng C. Y., Seabold G. K., Horak M. and Petralia R. S. (2011) MAGUKs, synaptic development, and synaptic plasticity. *Neuroscientist* **17**, 493–512.